Journal of Medicinal Chemistry

Brief Article

Discovery of the Second Generation ROR# Inhibitors Composed of an Azole Scaffold

Masayuki Kotoku, Takaki Maeba, Shingo Fujioka, Masahiro Yokota, Noriyoshi Seki, Keisuke Ito, Yoshihiro Suwa, taku ikenogami, Kazuyuki Hirata, Yasunori Hase, Yoshiaki Katsuda, Naoki Miyagawa, Kojo Arita, Kota Asahina, Masato Noguchi, Akihiro Nomura, Satoki Doi, Tsuyoshi Adachi, Paul Crowe, Haiyan Tao, Scott Thacher, Hiromasa Hashimoto, Takayoshi Suzuki, and Makoto Shiozaki

J. Med. Chem., **Just Accepted Manuscript** • DOI: 10.1021/acs.jmedchem.8b01567 • Publication Date (Web): 18 Feb 2019

ACS Publications

is published by the American Chemical Society. 1155 Sixteenth Street N.W., Washington, DC 20036

	Suzuki, Takayoshi; Kyoto Prefectural University of Medicine , Graduate School of Medical Science, Kyoto Prefectural University of Medicine Shiozaki, Makoto; JAPAN TOBACCO INC., Central Pharmaceutical Research Institute

Discovery of the Second Generation RORγ Inhibitors Composed of an Azole Scaffold

Masayuki Kotoku,*,†,⊥ Takaki Maeba,† Shingo Fujioka,† Masahiro Yokota,† Noriyoshi Seki,† Keisuke Ito,† Yoshihiro Suwa,† Taku Ikenogami,† Kazuyuki Hirata,†Yasunori Hase,† Yoshiaki Katsuda,§ Naoki Miyagawa,§ Kojo Arita,§ Kota Asahina,¶ Masato Noguchi,† Akihiro Nomura,† Satoki Doi,† Tsuyoshi Adachi,† Paul Crowe,‡ Haiyan Tao,‡ Scott Thacher,‡ Hiromasa Hashimoto,† Takayoshi Suzuki,⊥ and Makoto Shiozaki*,†

†Chemical Research Laboratories, §Biological Pharmacological Research Laboratories, ¶Drug Metabolism & Pharmacokinetics Research Laboratories, Central Pharmaceutical Research Institute, Japan Tobacco Inc., 1-1, Murasaki-cho, Takatsuki, Osaka, 569-1125, Japan

⊥Graduate School of Medical Science, Kyoto Prefectural University of Medicine, 1-5 Shimogamo-hangi-cho, Sakyo-ku, Kyoto 603-0823, Japan

‡Orphagen Pharmaceuticals, 11558 Sorrento Valley Road, Suite 4, San Diego, California, 92121, United States

KEYWORDS. RORγ, Autoimmune diseases, Th1, Th2, Th17, RORγ, CD3 challenge model, improved PK profiles, LogD

ABSTRACT: Starting from a previously reported RORγ inhibitor (**1**), successive efforts to improve *in vivo* potency were continued. Introduction of metabolically beneficial motifs in conjunction with scaffold hopping was examined, resulting in discovery of the second generation RORγ inhibitor composed of a 4-(isoxazol-3-yl)butanoic acid scaffold (**24**). Compound **24** achieved a 10-fold improvement in *in vivo* potency in a mouse CD3 challenge model along with significant anti-inflammatory effects in a mouse dermatitis model.

INTRODUCTION

In 2005, more than two decades after the discovery of Th1 and Th2 cells, the classical understanding of the helper T cell theory was revised and an early developmental pathway that diverged from the Th1 and Th2 lineages was confirmed as the Th17 lineage.[1,2] Although pre-Th1 cells are believed to be present and to take a part as common intermediates of Th1 and Th17 cells, Th17 cells were shown to arise directly from $CD4^+$ helper T cells in the presence of interleukin (IL)-23. These studies confirmed that three distinct lineages were initiated from effector $CD4^+$ helper T cells.[3] The new findings suggested that direct inhibition of Th17 cell differentiation and proliferation could be a rational approach for the treatment of autoimmune diseases, and several biologic medications blocking the Th17 cell function are currently under human clinical trials or have even been launched quite recently.[4-6]

Among molecules that participate in the Th17 signaling, RORγ has been widely recognized as a most attractive entity since it functions as a master regulator of Th17 cell development.[7] Various compounds targeting the orphan nuclear receptor have been reported,[8-16] but only a limited number of modulators of this target have progressed into human clinical trials. This drug discovery program has been challenged by the need to balance good potency, high specificity and favorable pharmacokinetic (PK) profiles. Recently, we identified a novel series of RORγ inhibitors. The lead compound suffered from poor metabolic stability as well as insufficient selectivity, but these characteristics were considerably improved during the course of the investigation.[17] Despite our improvements, the *in vivo*

potency of the best compound **1** was still unsatisfactory with an ED_{50} value of 30 mg/kg , which compelled us to pursue the generation of a more advanced inhibitor.

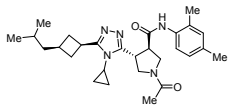

compd	EC_{50}[a] (μM)	LogD	MS[b] (%)	Caco2 Papp[c] (10^{-6} cm/sec)
1	0.034	4.3	61	20

Figure 1. Profiles of the first generation inhibitor **1**. [a]Human RORγ luciferase (LUC) assay. Values of EC_{50} are mean values determined from at least 3 replicates. Positive control OR-1050 showed EC_{50} value of 0.19 ±0.048 (mean ±SD), n=19.[18] [b]Metabolic stability (MS) in human liver microsomes after 60 minutes of incubation. Value is the remaining % of compound **1**. [c]Apparent permeability coefficients.

In the preceding paper, the drug-likeness properties represented by ligand efficiency (LE) and the fraction of sp^3 carbons (Fsp^3) attained their respective benchmark scores,[19,20] thus indicating another approach was needed to overcome the moderate *in vivo* potency. Herein, we report the successful efforts in our RORγ program focused on the improvement of PK profiles, which led to discovery of the second generation inhibitors composed of an azole scaffold.

RESULTS AND DISCUSSION

The ligand binding pocket of RORγ is heavily hydrophobic,[21] thus suggesting that an increase in *in vitro* potency could be theoretically achievable by accommodation of lipophilic motifs in the binding pocket. However, such a tactic may sacrifice metabolic stability of the ligand, therefore pursuing such van der Waals interactions was not a practical option in this case. Alternatively, implementation of a polar functionality outside the binding pocket is a viable strategy and a number of successful examples have been reported in the literature.[22,23] The X-ray co-crystal structure of our first generation inhibitor[17] suggested a substituent at the β-position of the propanoyl moiety would project toward the outside the pocket (Figure 2), so we introduced substituents bearing a functional group at the terminus and examined their effects on metabolic stability, as well as other pharmacokinetic parameters.

To conduct such modifications, compound **2**, a surrogate analogue of **1** served as a model compound in view of the synthetic tractability. Varieties of substituents allocating a functional group at the terminus were examined (Table 1), and the alkyl amines (**4**, **5**) as well as the alkanoic acid (**7**) were identified as effective boosters to improve metabolic stability. Unfortunately, their potencies, as measured by the LUC assay to determine EC_{50}, were significantly worse even though favorable binding was presumed based on the crystal structure of compound **1**. We hypothesized that factors other than the presence of the substituents themselves were hampering the accommodation of the new compounds in the binding pocket.

Table 1. Effects of R^1 Groups on Potency and ADME Profiles

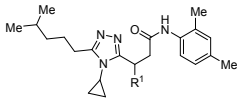

compd	R^1	EC_{50}[a] (μM)	LogD	MS[b] (%)	Caco2 Papp[c] (10^{-6} cm/sec)
2	H	1.7	3.9	27	36
3	$(CH_2)_2OH$	0.44	3.5	21	11
4	$(CH_2)_2NH_2$	>20	3.1	88	0.2
5	$(CH_2)_2NMe_2$	19	3.3	85	0.8
6	$(CH_2)_2NHAc$	11	3.5	39	1.3
7	$(CH_2)_2COOH$	>20	2.9	91	0.2
8	$(CH_2)_2CONH_2$	16	3.4	44	0.8
9	$(CH_2)_2CONHMe$	6.4	3.5	65	1.5
10	$(CH_2)_2CONMe_2$	2.7	3.8	45	7.0

[a]Values of EC_{50} are mean values determined from at least 3 replicates. Positive control OR-1050 showed EC_{50} value of 0.19 ±0.048 (mean ±SD), n=19.[18] [b]MS in human liver microsomes. [c]Apparent permeability coefficients. Compounds **3**–**10** are racemic.

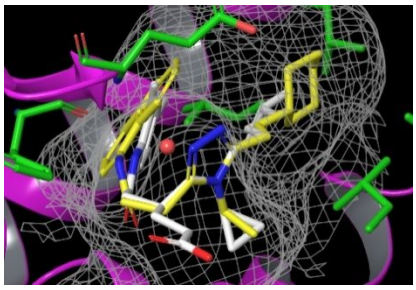

Figure 2. (A) Docking result of **7**. The docked **7** (white) was superimposed with a first generation RORγ inhibitor (yellow) in complex with RORγ (PDB code 5AYG).[24]

We undertook a systematic analysis of their physicochemical characteristics. If the nature of the binding pocket was taken into consideration, the lipophilicity of the compounds could affect the binding affinity toward RORγ. Actually, significant reduction of LUC potency was observed once LogD of these compounds fell below a threshold value (roughly 3.3), suggesting a possible cut-off value of lipophilicity to achieve good binding (Figure 3).

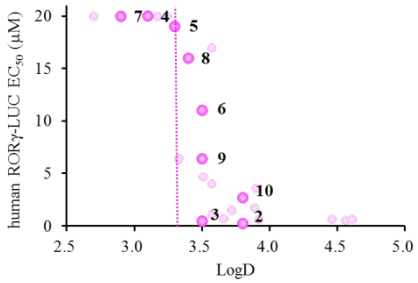

Figure 3. A threshold value of LogD. Light pink dots represent other close congeners whose structure and profiles were listed in the section of supporting information.

Driven by such a speculation, we decided to synthesize more lipophilic analogues bearing the propanoic acid substituent, the most metabolically beneficial substituent listed in Table 1. Initially, compound **11** composed of an isoxazole scaffold was synthesized, in which the ethylene motif as well as the aniline part were simultaneously modified with an aim to minimize plausible metabolic sites. As expected, **11** showed an increased LogD, exceeding the hypothetical cut-off value. This compound displayed both decent LUC potency and good metabolic stability. We became confident that 4-(isoxazole-3-yl)butanoic acid is a desirable platform, and further optimization of **11** was conducted to identify the second generation RORγ inhibitors composed of an azole core scaffold.

To improve the potency of **11** as measured by the LUC assay, we focused on the benzene part on the central isoxazole core. Based on the previous exploration, this location was considered to favor a flattened architecture, so a set of smaller-sized aromatic compounds were examined as benzene alternates. As shown in Table 2, various heterocycles were applied and isoxazole derivatives (**12**, **13**) showed improved LUC potency while the transformation to the 2, 5-disubstituted oxazole (**14**) or thiazole (**15**) resulted in significant reductions of the potency. Given the hydrophobic nature of the pocket, several subsites in the pocket were presumed to disfavor a polar environment, and we observed a tendency that the presence of a hetero atom led to reduction of the potency. Additionally, two regioisomeric thiazole analogues (**16**, **17**) showed contrasting outcomes in LUC potency. The terminal isobutyl group of each compound must project toward a different location due to the presence of a longer bond length, particularly the C-S bond, and the terminal substituent of **16** was likely positioned at the mismatched site while **17** allocated the same substituent at the right location.

Once the 3, 5-disubstituted isoxazole was identified as a favorable motif for the Ar part with the best balance between LUC potency and metabolic stability, the final optimization was conducted with **12** by modulating both terminal substituents (Table 3). Firstly, an additional carbon atom was introduced at the isobutyl moiety, and a slight increase in LUC potency was observed regardless of the difference in the location (**21**, **23**). In order to further improve metabolic stability, halogen atoms were incorporated. A simple fluorination of the substituents on the isoxazole had virtually no effect on the stability (**20**, **22** and **25**), while di-halo-anilide analogues showed better metabolic stability (**24**, **26** and **27**).

Table 2. Discovery of a Potent and Metabolically Stable Scaffold

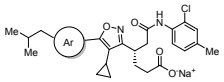

compd	Ar	EC_{50}[b] (μM)	LogD	MS[c] (%)	Caco2 Papp[d] (10^{-6} cm/sec)
11[a]		0.044	4.8	80	16
12		0.014	3.9	74	36
13		0.012	3.8	54	28
14		0.66	3.7	75	32
15		0.12	4.0	82	28
16		3.8	3.8	82	34
17		0.017	3.8	54	34
18		0.062	3.6	90	25
19		0.056	3.4	78	10

[a]Salt-free form. [b]EC_{50} are mean values determined from at least 3 replicates. Positive control OR-1050 showed EC_{50} value of 0.19 ±0.048 (mean ±SD), n=19.[18] [c]MS in human liver microsomes. [d]Apparent permeability coefficients.

Table 3. Optimization of Terminal Substituents

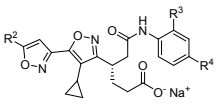

compd	R^2	R^3	R^4	EC_{50}[a] (μM)	LogD	MS[b] (%)
20	Me_2CHCF_2	Cl	Me	0.007	4.0	74
21	$Me_2CHCH_2CH_2$	Cl	Me	0.008	4.3	79
22	$Me_2CHCH_2CF_2$	Cl	Me	0.008	4.4	78
23	Me_3CCH_2	Cl	Me	0.007	4.2	84
24	Me_3CCH_2	Cl	Cl	0.009	4.2	96
25	Me_3CCF_2	Cl	Me	0.006	4.3	77
26	Me_3CCF_2	Cl	F	0.006	4.0	90
27	Me_3CCF_2	F	Cl	0.007	4.2	107

[a]Values of EC_{50} are mean values determined from at least 3 replicates. Positive control OR-1050 showed EC_{50} value of 0.19 ±0.048 (mean ±SD), n=19.[18] [b]MS in human liver microsomes.

Since the LUC potency and the metabolic stability had been improved by our modifications to the first generation structure **1**, we selected compound **24** to conduct *in vivo* studies. Firstly, the experimental allergic encephalomyelitis (EAE) model was selected to assess the pharmacodynamic (PD) effects of **24** since Th17-derived IL-17 is recognized as a major mediator in EAE. Mice were immunized by an addition of myelin oligodendrocyte glycoprotein (MOG), complete Freund's adjuvant and pertussis toxin (PTX), then IL-17 production was further boosted by restimulation with anti-CD3 antibody.[17] At 8 h after the oral administration, the plasma IL-17 level of each mouse was analyzed and dose-dependent suppression of IL-17 production was observed

(Figure 4A). The ED_{50} value of **24** was calculated as 3 mg/kg, achieving roughly a 10-fold improvement in comparison to **1** in this pharmacodynamic (PD) model. To further confirm the value of this compound, disease-modifying effects were evaluated in the IL-23-induced mouse dermatitis model.[25,26] Dermal inflammation was induced by IL-23 injection, and mice were subjected to multiple oral dosing once daily for eleven days. The ear thickness of each mouse was measured on day 1, 5, 8, 10 and 12, and significant reduction of ear swelling was observed for compound treatment groups (Figure 4B).

(A)

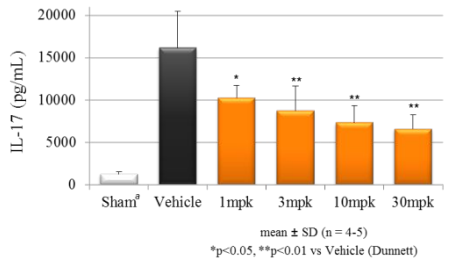

(B)

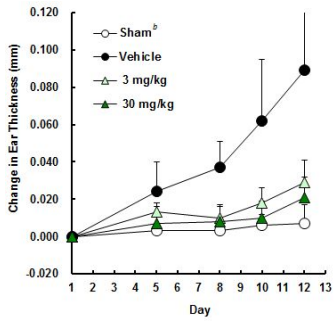

Figure 4. Effect of compound **24** in (A) CD3-induced mouse PD model. [a]Non-immunized (neither MOG nor complete Freund's adjuvant nor PTX treatment) group. (B) IL-23-induced mouse dermatitis model. [b]Non-IL-23-treatment group.

High RORγ specificity of **24** was also confirmed by the absence of inhibitory activity against other nuclear receptors (EC_{50}>20 μM; hRORα, mLXR, hRXR, hPPARδ, hPPARγ) and the lack of time-dependent CYP inhibition properties (IC_{50}>50 μM; hCYP3A4m, hCYP3A4t, hCYP2C9, hCYP2D6, hCYP1A2, hCYP2C19). Compound **24** showed greatly improved PK profiles compared to our first generation inhibitors (Table 4), suggesting it was indeed a promising preclinical candidate as a selective RORγ inhibitor.

Table 4. PK parameters of 24 in rats

iv parameters (1.0 mg/kg)			po parameters (3.0 mg/kg)		
$t_{1/2\beta}$ (h)	Cl_{tot}[a] (L/h/kg)	Vd_{ss}[b] (L/kg)	AUC[c] (μM•h)	MRT[d] (h)	F[e] (%)
4.2	0.25	0.76	15	4.9	72.0

[a]Total body clearance. [b]Volume of distribution at steady state. [c]Area under the curve. [d]Mean residence time. [e]Bioavailability.

RORγ inhibitors reported in this manuscript were prepared according to Scheme 1. Regarding compounds bearing a 1,2,4-triazole core, the method was almost identical to the one previously reported[17] except for including extra processes for pendant group modifications. Meanwhile, the second generation RORγ inhibitors typified by the isoxazole core structure were synthesized through alkynones or 4-cyclopropyl-3,5-di-alkylated ioxazoles, which we believe is an efficient strategy for synthesizing fully-substituted isoxazoles in a regio-selective manner.[27]

Scheme 1. Synthesis of Compounds 3-27

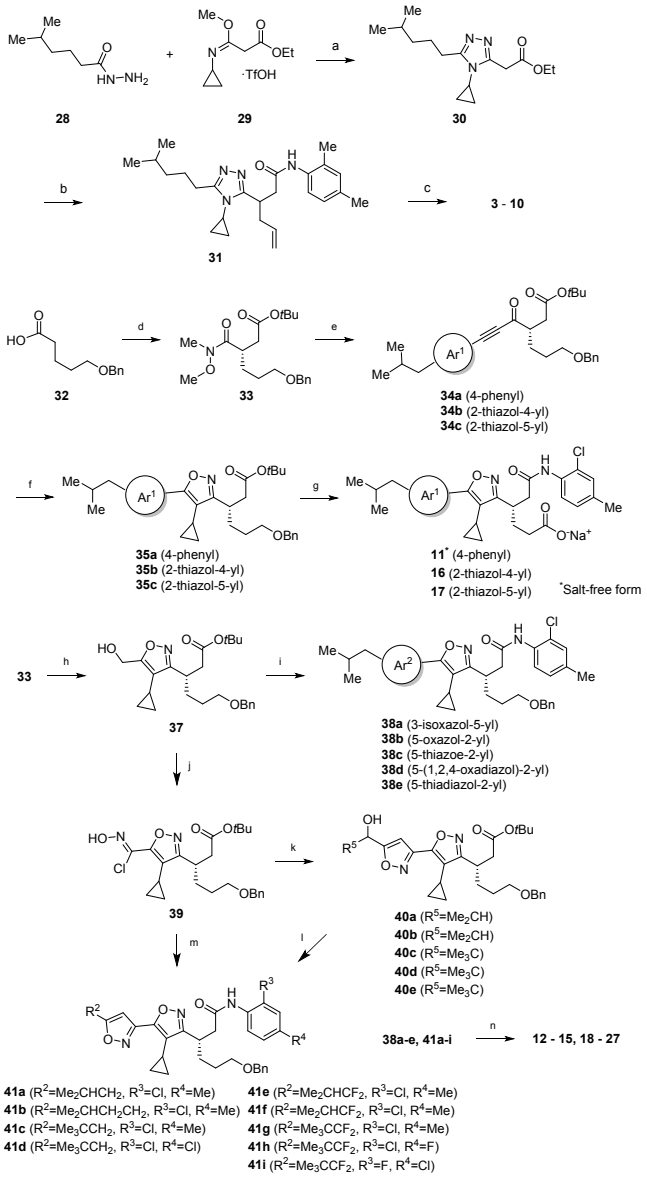

Reagents and conditions: (a) Et_3N, 1,4-dioxane; (b) (i) *tert*-butyl bromoacetate, NaH, THF; (ii) allyl iodide, NaHMDS, THF; (iii) 4 M NaOH, EtOH; (iv) TFA, $CHCl_3$, MeCN; (v) 2,4-dimethylaniline, HATU, Et_3N, DMF; (c) see supporting information for detailed protocol to introduce respective functional groups. (d) (i) (*R*)-4-benzyloxazolidin-2-one, WSC•HCl, DMAP, MeCN; (ii) LDA, *tert*-butyl bromoacetate,

THF; (iii) H_2O_2, 4M LiOH, THF; (iv) (*R*)-1-phenylethan-1-amine, MTBE; (v) $KHSO_4$, EtOAc, H_2O; (vi) MeONHMe•HCl, WSC•HCl, HOBt•H_2O, *i*-Pr_2NEt, MeCN; (e) aryl alkyne, *n*-BuLi, THF; (f) (i) $MeONH_2$•HCl, Na_2CO_3, EtOH; (ii) ICl, CH_2Cl_2; (iii) cyclopropylboronic acid pinacol ester, K_3PO_4, $PdCl_2(PPh_3)_2$, DMF; (g) (i)H_2, $Pd(OH)_2$/C, MeOH, THF; (ii) TEMPO, $NaClO_2$, NaClO, MeCN, phosphate buffer (pH 6.8); (iii) MeI, K_2CO_3, DMF; (iv) TFA, $CHCl_3$; (v) $SOCl_2$, 2-chloro-4-methyl aniline, DMA; (vi) 2M NaOH, MeOH, THF; (h) (i) *i*-Bu_2AlH, toluene, THF; (ii) H_2NOH•HCl, 4M NaOH, EtOH, THF, H_2O; (iii) NCS, DMF, toluene; (iv) 3-bromoprop-2-yn-1-ol, K_2CO_3, toluene, H_2O; (v) cyclopropylboronic acid pinacol ester, K_3PO_4, $PdCl_2(PPh_3)_2$, DMF; (i) see supporting information for detailed protocol to construct the Ar^2 moiety, heteroaromatic rings; (j) (i) DMP, $CHCl_3$; (ii) NH_2OH•HCl, 4M NaOH, EtOH, THF, H2O; (iii) NCS, DMF; (k) alkyl alkyne-3-ol, K_2CO_3, toluene, H_2O; (l) (i) DMP, $CHCl_3$; (ii) Deoxo-Fluor®, CH_2Cl_2; (iii) TFA, toluene; (iv) $SOCl_2$, 2,4-disubstituted aniline, DMA; (m) (i) alkyl alkyne, K_2CO_3, toluene, H_2O; (ii) TFA, toluene; (iii) 2,4-disubstituted aniline, HATU, *i*-Pr_2NEt, DMF; (n) (i) BBr_3, CH_2Cl_2; (ii) TEMPO, $NaClO_2$, NaClO, MeCN, phosphate buffer (pH 6.8); (iii) 2M NaOH, EtOH.

The binding conformation of **24** in RORγ was subsequently confirmed by the X-ray co-crystal analysis, in which the metabolically beneficial carboxylate was proven to project outside the pocket as originally expected (Figure 5).

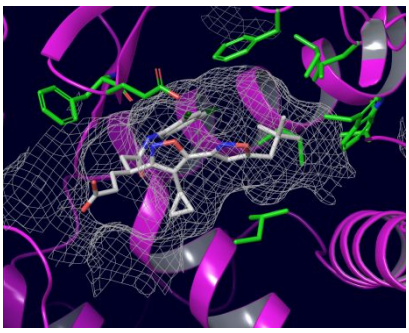

Figure 5. Cocrystal structure of **24** in RORγ (PDB code 6IVX).

CONCLUSION

We have identified potent and metabolically stable RORγ inhibitors composed of an isoxazole scaffold. In order to overcome a general shortcoming of RORγ inhibitors, their poor metabolic stability, we strategized to introduce metabolically beneficial functionalities at the outside of the binding pocket. Although our first generation RORγ inhibitors were not compatibility to such pendant groups, those isoxazole analogues realized good potency as well as high metabolic stability. Furthermore, the representative compound **24** was proven to achieve both high RORγ specificity and improved *in vivo* potency. Compound **24** is expected to be an ideal probe to accelerate the future research of RORγ pharmacology.

EXPERIMENTAL SECTION

General. The purity of all of the tested compounds was determined by HPLC (SHIMADZU Prominence) and was > 95%. The chemistry, experimental information and spectroscopic data for the target compounds were supplied in the Supporting Information. The representative procedure of the final transformation to afford the target compounds was presented as exemplified by the synthesis of **24**.

Sodium (*S*)-4-(4'-cyclopropyl-5-neopentyl-[3,5'-biisoxazol]-3'-yl)-6-((2,4-dichlorophenyl)amino)-6-oxohexanoate (**24**)

To a solution of **41d** (264 mg, 0.432 mmol) in CH_2Cl_2 (4.0 mL) was added 1.0 M BBr_3 in CH_2Cl_2 (1.1 mL, 1.08 mmol) dropwise at –78 °C. The reaction mixture was warmed to room temperature over 20 min and stirred for another 10 min. Saturated aqueous $NaHCO_3$ was added to the reaction at 0 °C and extracted with EtOAc. The organic layer was washed with brine, and then dried over Na_2SO_4. After filtration and removal of the solvent under reduced pressure, the residue was purified by flash chromatography (EtOAc:*n*-hexane = 1:4 to 1:1 (v/v)). To a solution of the debenzylated compound (180 mg, 0.346 mmol) in MeCN (1.3 mL) and 1.0 M phosphate buffer (pH=6.8, 1.3 mL) were added TEMPO (5.4 mg, 0.0346 mol) and NaClO2 (78 mg, 0.692 mmol). Sodium hypochlorite solution (90 µL) was added dropwise to the reaction mixture at 0 °C and stirred at room temperature for 1 h. The reaction mixture was quenched with 20% aqueous Na_2SO_3 at 0 °C and extracted with EtOAc. The organic layer was washed with 1M HCl, water and brine, and then dried over Na_2SO_4. After filtration and removal of the solvent under reduced pressure, the residue was purified by preparative TLC ($CHCl_3$:MeOH = 12:1 (v/v)) to give the corresponding carboxylic acid (161 mg, 70 % yield). To a solution of this compound (161 mg, 0.302 mmol) in EtOH (1.0 mL) was added 1 M NaOH (302 µL, 0.302 mmol). After stirring at room temperature for 30 min, the reaction mixture was concentrated under reduced pressure to give the title compound **24** (168 mg, quantitative).

^{1}H NMR (400 MHz,DMSO-d_6) δ: 0.43–0.55 (m, 1H), 0.59–0.72 (m, 1H), 0.85–1.02 (m, 2H), 0.95 (s, 9H), 1.67–1.78 (m, 1H), 1.78–1.98 (m, 4H), 2.76 (s, 2H), 2.82 (dd, J = 15.20, 6.80Hz, 1H), 2.90 (dd, J = 15.20, 8.40Hz, 1H), 3.47–3.59 (m, 1H), 6.73 (s, 1H), 7.34 (dd, J = 8.80, 2.40Hz, 1H), 7.59 (d, J = 2.40Hz, 1H), 7.61 (d, J = 8.80Hz, 1H), 10.03 (brs, 1H). HRMS m/z: $[M–Na+2H]^+$ calcd for $C_{26}H_{30}N_3O_5Cl_2$, 534.1557; found, 534.1555. HPLC purity: 97.2 %. $[\alpha]^{20}_D$ -2.5 (c 0.40, MeOH).

CD3-induced mouse PD model[17]

Peptides derived from myelin oligodendrocyte glycoprotein ($MOG_{35–55}$) were dissolved in D-PBS (–) at concentration of 3 mg/mL, and then emulsified with an equal volume of complete Freund's adjuvant. Female C57BL/6 mice were immunized with the MOG35–55 emulsion by subcutaneous injection at two sites on the back (75 µg of $MOG_{35–55}$ per site) and 0.2 µg/200 µL of pertussis toxin (PTX) in D-PBS (–) was injected intraperitoneally on day 1. On day 3, the same amount of PTX was injected. On day 5, 1 µg / 200 µL of the anti-CD3 antibody dissolved in saline was injected intravenously to induce IL-17 production. The blood samples

were collected 2 hours after the CD3 injection, then the IL-17A level in plasma was measured by ELISA. The test article was administered orally 3 h or 8 h before the CD3 antibody injection into 5 mice per each group.

IL-23-induced dermatitis model[25,26]

Intradermal injections of 250 ng recombinant mouse IL-23 (R&D Systems, Minneapolis, MN) in 20 μL PBS containing 0.1% BSA were performed into the left ear of anesthetized mice on days 1, 3, 5, 8 and 10. Compound **24** (3 and 30 mg/kg) or 0.5% MC were administered orally at a volume of 10 mL/kg every day from day 1 to 11. On Days 1, 5, 8, 10 and 12, the left ear thickness was measured using a digital thickness gauge (Digimatic Indicator IDA-112M, Mitutoyo Corporation, Kawasaki, Japan). The increase in the ear thickness from baseline value (the ear thickness on Day 1) was defined as the change in the ear thickness.

ASSOCIATED CONTENT

Supporting Information

The Supporting information is available free of charge on the ACS Publications website at DOI:
Synthetic procedures, experimental data, docking protocol, assay procedures and PK profiles of **24** (PDF)
Molecular formula strings (CSV)

AUTHOR INFORMATION

Corresponding Author

*For M.K.: E-mail, masayuki.kotoku@jt.com
*For M.S.: E-mail, makoto.shiozaki@jt.com

ORCID

Masayuki Kotoku: 0000-0003-2245-1673
Makoto Shiozaki: 0000-0001-5519-6547

Funding Sources

The authors declare no competing financial interest.

ABBREVIATIONS

RORγ, retinoic acid receptor-related orphan receptor gamma; ADME, absorption, distribution, metabolism, excretion; CYP, cytochrome P450; LXR, liver X receptor; RXR, retinoid X receptor; PPAR, peroxisome proliferator activated receptor; DMP, Dess-Martin periodinane; TEMPO, 2,2,6,6-tetramethylpiperidine 1-oxyl; HATU, 1-[bis(dimethylamino)methylene]-1H-1,2,3-triazolo[4,5-b]pyridinium 3-oxide hexafluorophosphate; TfOH, trifluoromethanesulfonic acid.

REFERENCES

1) Harrington, L. E.; Hatton, R. D.; Mangan, P. R.; Turner, H.; Murphy, T. L.; Murphy, K. M.; Weaver, C. T. Interleukin 17-producing $CD4^+$ effector T cells develop via a lineage distinct from the T helper type 1 and 2 lineages. *Nat. Immunol.* **2005**, *6*, 1123– 1132.
2) Park, H.; Li, Z.; Yang, X. O.; Chang, S. H.; Nurieva, R.; Wang, Y.-H.; Wang, Y.; Hood, L.; Zhu, Z.; Tian, Q.; Dong, C. A distinct lineage of CD4 T cells regulates tissue inflammation by producing interleukin 17. *Nat. Immunol.* **2005**, *6*, 1133– 1141.
3) Wynn, T. A. TH-17: a giant step from TH1 and TH2. *Nat. Immunol*. **2005**, *6*, 1069– 1070.
4) Langley, R. G.; Elewski, B. E.; Lebwohl, M.; Reich, K.; Griffiths, C. E.; Papp, K.; Puig, L.; Nakagawa, H.; Spelman, L.; Sigurgeirsson, B.; Rivas, E.; Tsai, T. F.; Wasel, N.; Tyring, S.; Salko, T.; Hampele, I.; Notter, M.; Karpov, A.; Helou, S.; Papavassilis, C.; ERASURE study group; FIXTURE study group. Secukinumab in plaque psoriasisresults of two phase 3 trials. *N. Engl. J. Med*. **2014**, *371*, 326–338.
5) Griffiths C. E.; Reich K.; Lebwohl M.; van de Kerkhof P.; Paul C.; Menter A.; Cameron G. S.; Erickson J.; Zhang L.; Secrest R. J.; Ball S.; Braun D. K.; Osuntokun O. O.; Heffernan M. P.; Nickoloff B. J.; Papp K.; UNCOVER-2 and UNCOVER-3 investigators. Comparison of ixekizumab with etanercept or placebo in moderate-tosevere psoriasis (UNCOVER-2 and UNCOVER-3): results from two phase 3 randomised trials. *Lancet* **2015**, *386*, 541–551.
6)Lebwohl, M.; Strober, B.; Menter, A.; Gordon, K.; Weglowska, J.; Puig, L.; Papp, K.; Spelman, L.; Toth, D.; Kerdel, F.; Armstrong, A. W.; Stingl, G.; Kimball, A. B.; Bachelez, H.; Wu, J. J.; Crowley, J.; Langley, R. G.; Blicharski, T.; Paul, C.; Lacour, J. P.; Tyring, S.; Kircik, L.; Chimenti, S.; Callis, Duffin, K.; Bagel, J.; Koo, J.; Aras, G.; Li, J.; Song, W.; Milmont, C. E.; Shi, Y.; Erondu, N.; Klekotka, P.; Kotzin, B.; Nirula, A. Phase 3 studies comparing Brodalumab with Ustekinumab in psoriasis. *N. Engl. J. Med*. **2015**, *373*, 1318–1328.
7) Ivanov, I. I.; McKenzie, B. S.; Zhou, L.; Tadokoro, C. E.; Lepelley, A.; Lafaille, J. J.; Cua, D. J.; Littman, D. R. The orphan nuclear receptor RORγt directs the differentiation program of proinflammatory IL-17^+ T helper cells. *Cell* **2006**, *126*, 1121– 1133.
8)Cyr, P.; Bronner, S. M.; Crawford, J. J. Recent progress on nuclear receptor RORγ modulators. *Bioorg. Med. Chem. Lett*. **2016**, *26*, 4387-4393.
9) Kummer, D. A.; Cummings, M. D.; Abad, M.; Barbay, J.; Castro, G.; Wolin, R.; Kreutter, K. D.; Maharoof, U.; Milligan, C.; Nishimura, R.; Pierce, J.; Schalk-Hihi, C.; Spurlino, J.; Urbanski, M.; Venkatesan, H.; Wang, A.; Woods, C.; Xue, X.; Edwards, J. P.; Fourie, A. M.; Leonard, K. Identification and structure activity relationships of quinoline tertiary alcohol modulators of RORγt. *Bioorg. Med. Chem. Lett*. **2017**, *27*, 2047-2057.
10) Kono, M.; Ochida, A.; Oda,T.; Imada, T.; Banno, Y.; Taya, N.; Masada, S.; Kawamoto, T.; Yonemori, K.; Nara, Y.; Fukase, Y.; Yukawa, T.; Tokuhara, H.; Skene, R.; Sang, B. C.; Hoffman, I. D.; Snell, G. P.; Uga, K.; Shibata,A.; Igaki, K.; Nakamura, Y.; Nakagawa, H.; Tsuchimori, N.; Yamasaki, M.; Shirai, J.; Yamamoto, S. Discovery of [*cis*-3-({(5*R*)-5-[(7-Fluoro-1,1-dimethyl-2,3-dihydro-1*H*-inden-5-yl)carbamoyl]-2-methoxy-7,8-dihydro-1,6-naphthyridin-6(5*H*)-yl}carbonyl)cyclobutyl]acetic acid (TAK-828F) as a potent, selective, and orally available novel retinoic acid receptor-related orphan receptor γt inverse agonist. *J. Med. Chem.* **2018**, *61*, 2973-2988.
11) (a) Fauber, B. P.; René, O.; Burton, B.; Everett, C.; Gobbi, A.; Hawkins, J.; Johnson, A. R.; Liimatta, M.; Lockey, P.; Norman, M.; Wong, H. Identification of tertiary sulfonamides as RORc inverse agonists. *Bioorg. Med. Chem. Lett*. **2014**, *24*, 2182–2187. (b) Fauber, B. P.; René, O.; de Leon Boenig, G.; Burton, B.; Deng, Y.; Eidenschenk, C.; Everett, C.; Gobbi, A.; Hymowitz, S. G.; Johnson, A. R.; La, H.; Liimatta, M.; Lockey, P.; Norman, M.; Ouyang, W.; Wang, W.; Wong, H. Reduction in lipophilicity improved the solubility, plasma–protein binding, and permeability of tertiary

sulfonamide RORc inverse agonists. *Bioorg. Med. Chem. Lett*. **2014**, *24*, 3891– 3897.
12) Narjes, F.; Xue, Y.; von Berg, S.; Malmberg, J.; Llinas, A.; Olsson, R. I.; Jirholt, J.; Grindebacke, H.; Leffler, A.; Hossain, N.; Lepistö, M.; Thunberg, L.; Leek, H.; Aagaard, A.; McPheat, J.; Hansson, E. L.; Bäck, E.; Tångefjord, S.; Chen, R.; Xiong, Y.; Hongbin, G.; Hansson, T. G. Potent and orally bioavailable inverse agonists of RORγt resulting from structure-based design. *Bioorg. J. Med. Chem*. **2018**, *61*, 7796–7813.
13) Pandya, V. B.; Kumar, S.; Rajiv, S.; Desai, R. C. Combating autoimmune diseases with retinoic acid receptor-related orphan receptor-γ (RORγ or RORc) inhibitors: Hits and misses. *J. Med. Chem*. **2018**, *61*, 10976– 10995.
14) Gong, H.; Weinstein, D. S.; Lu, Z.; Duan, J. J.; Stachura, S.; Haque, L.; Karmakar, A.; Hemagiri, H.; Raut, D. K.; Gupta, D. K.; Khan, J.; Camac, D.; Sack, J. S.; Pudzianowski, A.; Wu, D. R.; Yarde, M.; Shen, D. R.; Borowski. V.; Xie, J. H.; Sun, H.; D'Arienzo, C.; Dabros, M.; Galella, M. A.; Wang, F.; Weigelt, C. A.; Zhao, Q.; Foster, W.; Somerville, J. E.; Salter-Cid, L. M.; Barrish, J. C.; Carter, P. H.; Dhar, T. G. M. Identification of bicyclic hexafluoroisopropyl alcohol sulfonamides as retinoic acid receptor-related orphan receptor gamma (RORγ/RORc) inverse agonists. Employing structure-based drug design to improve pregnane X receptor (PXR) selectivity. *Bioorg. Med. Chem. Lett*. **2018**, *28*, 85-93.
15) Enyedy, I. J.; Powell, N. A.; Caravella, J.; van Vloten, K.; Chao, J.; Banerjee, D.; Marcotte, D.; Silvian, L.; McKenzie, A.; Hong, V. S.; Fontenot, J. D. Discovery of biaryls as RORγ inverse agonists by using structure-based design. *Bioorg. Med. Chem. Lett*. **2016**, *26*, 2459–2463.
16) Schnute, M. E.; Wennerstål, M.; Alley, J.; Bengtsson, M.; Blinn. J. R.; Bolten, C. W.; Braden, T.; Bonn, T.; Carlsson, B.; Caspers, N.; Chen, M.; Choi, C.; Collis, L.P.; Crouse, K.; Färnegårdh, M.; Fennell, K.F.; Fish, S.; Flick, A.C.; Goos-Nilsson, A.; Gullberg, H.; Harris, P.K.; Heasley, S.E.; Hegen, M.; Hromockyj, A. E.; Hu, X.; Husman, B.; Janosik. T.; Jones, P.; Kaila, N.; Kallin, E.; Kauppi, B.; Kiefer, J. R.; Knafels, J.; Koehler, K.; Kruger, L.; Kurumbail, R. G.; Kyne, R. E. Jr.; Li. W.; Löfstedt, J.; Long, S. A.; Menard, C. A.; Mente, S.; Messing, D.; Meyers, M.J.; Napierata, L.; Nöteberg, D.; Nuhant, P.; Pelc, M. J.; Prinsen, M. J.; Rhönnstad; P.; Backström-Rydin, E.; Sandberg, J.; Sandström, M.; Shah, F.; Sjöberg, M.; Sundell, A.; Taylor, A. P.; Thorarensen, A.; Trujillo, J. I.; Trzupek, J. D.; Unwalla, R.; Vajdos, F. F.; Weinberg, R. A.; Wood, D. C.; Xing, L.; Zamaratski, E.; Zapf, C. W.; Zhao, Y.; Wilhelmsson, A.; Berstein, G. Discovery of 3-cyano-N-(3-(1-isobutyrylpiperidin-4-yl)-1-methyl-4(trifluoromethyl)-1H-pyrrolo[2,3-b]pyridin-5-yl)benzamide: A potent, selective, and orally bioavailable retinoic acid receptor-related orphan receptor C2 inverse agonist. *J. Med. Chem*. **2018**, *61*, 10415– 10439.
17) Hirata, K.; Kotoku, M.; Seki, N.; Maeba, T.; Maeda, K.; Hirashima, S.; Sakai, T.; Obika, S.; Hori, A.; Hase, Y.; Yamaguchi, T.; Katsuda, Y.; Hata, T.; Miyagawa, N.; Arita, K.; Nomura, Y.; Asahina, K.; Aratsu, Y.; Kamada, M.; Adachi, T.; Noguchi, M.; Doi, S.; Crowe, P.; Bradley, E.; Steensma, R.; Tao, H.; Fenn, M.; Babine, R.; Li, X.; Thacher, S.; Hashimoto, H.; Shiozaki, M. SAR exploration guided by LE and Fsp3: Discovery of a selective and orally efficacious RORγ inhibitor. *ACS Med. Chem. Lett*. **2016**, *7*, 23–27.
18) Thacher, S.; Li, X.; Babine, R.; Tse, B. Modulators of retinoid-related orphan receptor gamma. US Patent US8389739, 2013.
19) Abad-Zapatero, C. Ligand efficiency indices for effective drug discovery. *Expert Opin. Drug Discovery* **2007**, *2*, 469– 488.
20) Lovering, F.; Bikker, J.; Humblet, C. Escape from flatland: increasing saturation as an approach to improving clinical success. *J. Med. Chem*. **2009**, *52*, 6752– 6756.
21) Jin, L.; Martynowski, D.; Zheng, S.; Wada, T.; Xie, W.; Li, Y. Structural basis for hydroxycholesterols as natural ligands of orphan nuclear receptor RORc. *Mol. Endocrinol*. **2010**, *24*, 923–929.
22) Harikrishnan, L. S.; Warrier, J.; Tebben, A. J.; Tonukunuru, G.; Madduri, S. R.; Baligar, V.: Mannoori, R.; Seshadri, B.; Rahaman, H.; Arunachalam, P. N.; Dikundwar, A. G.; Fink, B. E.; Fargnoli, J.; Fereshteh, M.; Fan, Y.; Lippy, J.; Ching-Ping Ho, C. P.; Wautlet, B.; Borzilleri, R. M. Heterobicyclic inhibitors of transforming growth factor beta receptor I (TGFβRI). *Bioorg. Med. Chem*. **2018**, *26*, 1026-1034.
23) Rodrigues, D. A.; Pinheiro, P. S. M.; Ferreira, T. T. S. C.; Thota, S; Fraga, C. A. M. Structural basis for the agonist action at free fatty acid receptor 1 (FFA1R or GPR40). *Chem. Biol. Drug. Des*. **2018**, *91*, 668–680.
24) The structure of compound **7** was optimized using MacroModel from Schrödinger Suite 2018 and docked into RORγ-compound **1** crystal structure by superimposing with triazole part of **1**.
25) Mabuchi T, Takekoshi T, Hwang S. T. Epidermal CCR6+ γδ T cells are major producers of IL-22 and IL-17 in a murine model of psoriasiform dermatitis. *J Immunol*. **2011**, *187*, 5026-5031.
26) Arita, K.; unpublished results
27) Crossley, J. A.; Browne, D. L. An alkynyliodide cycloaddition strategy for the construction of iodoisoxazoles. *J. Org. Chem*. **2010**, *75*, 5414–5416.

Table of Contents Graphic